3

Wideband 20-Element 3D-MIMO Antenna for Localization System

*In this chapter, a low-profile wideband quad-element MIMO antenna with high isolation is designed, which is utilized to propose a 20-element MIMO antenna. Each element of the MIMO antenna covers a wideband occupying a small area. The orthogonal symmetric arrangement of a single antenna forms an extremely compact quad-element MIMO antenna having shared ground plane. The proposed antenna has a -10 dB ($S_{ij} \in i=j$) impedance bandwidth of 77.52% (3.95-8.95 GHz) and a minimum isolation ($S_{ij} \in i \neq j$) value of 17 dB. The measured and simulated results are found in good agreement that confirms the proposed antenna is appropriate for extending a higher-order MIMO system. Further, a low-profile quad-element MIMO antennas is arranged orthogonally at the four-corners and a quad-element MIMO antenna at the centre of, forms a 20-element MIMO antenna. It can be utilized in a localization system where different user's devices are connected to the primary host **

*Parts of this chapter have been published: Arun Kumar Saurabh and Manoj Kumar Meshram, "Wideband 20-elements 3D-MIMO antenna for localization system," *IEEE Transactions on Circuits and systems II: Express Briefs,* vol. 69, no. 2, pp. 409-413, 2022.

3.1 Introduction

Localization systems have become a common application since the Global Positioning System (GPS) has been commercialized. These GPS applications, however, do not work within indoor environments; thus, Indoor Positioning Systems (IPS) with similar properties, i.e., low cost and high localization accuracy, have become the attention of the research. Just like GPS, the most popular solutions for indoor positioning systems are essential based on radio frequency (RF) communication. To fulfil the purpose of the indoor localization system from the perspective of the antenna, different user's devices are communicated to the primary host. Therefore, the wideband high-order MIMO antenna may be utilized as a host device, where wideband technologies can be used in numerous functions of application as cellular, satellite, GPS, Bluetooth, Wi-Fi, WiMAX, WLAN, and WPAN, along with 5G. The primary concern is that Wi-Fi band-based technology is utilized in numerous user's devices, which are confined to the data rate and connections with other hosts. The capacity of power emission (75 nW/MHz) is fixed in ultra-wideband [111]. The wideband MIMO technology can also be utilized in indoor localization systems and wireless personal area networks (WPAN) based applications as the voice-controlled virtual portable assistant (Echo Dot, Google Home), smart home automation, smart office, smart classroom, intelligent vehicular network, etc. [111].

The consumer's demand for compact/low-profile/portable wireless devices increases due to the limited space available inside the equipment to embed the antenna elements [112]. Therefore, antenna elements should be more compact, low-profile, and closely placed. Due to this the correlation between antenna elements is high, and hence the MIMO antenna performances degrade. However, to design an extremely compact/low-profile MIMO antenna along with low coupling throughout wideband compared to narrowband is a highly challenging act for the designers.

To overcome from this issue, many decoupling techniques have been reported in the recent literature. The orthogonal placement of antenna elements were mostly reported to achieve inherent isolation [71]-[75], [79]-[80], [112]-[115]. The polarization diversity technique was utilized for low coupling [79]. Metalized walls and metal vias were used to improve the isolation between closely spaced elements [74]. Split-ring resonators (SRR) and complementary split-ring resonators (CSRR) were proposed to enhance the isolation [71], [116]. Stepped-slot based defected ground structures (DGS) were utilized for decoupling [70]. Discrete mushrooms like loading with the substrate integrated cavity-backed slot (SICBS) based technique was used for high isolation between closely spaced elements [96]. The low coupling was achieved using dual-layer electromagnetic bandgap (EBG) structure based on slow-wave technique [117]. T-shaped slot in the radiator and stub on the ground were used for mutual coupling cancellation [21]. T-shaped parasitic element in between two radiators and grounded stub branches were loaded for isolation enhancement [118]. Metamaterial-based superstrate was utilized for high isolation between closely spaced antenna element [102]. Metamaterial structure was loaded between two antenna elements for high isolation [105]. However, the above-discussed isolation techniques are mostly increasing the complexity, excluding the orthogonal placement technique. Therefore, without any decoupling network to achieve low coupling in designing an extremely compact/low-profile MIMO antenna is one of the presented proposal novelties.

In this chapter, an extremely compact/low-profile stub-loaded wideband quad-element MIMO antenna is utilized to configure a 20-element 3D-MIMO system for a localization system. The performances of the quad-element MIMO antenna are satisfactory. Thereby, it is used for extending the higher-order MIMO system. The four quad-element MIMO antenna are placed orthogonally at the corner of a quad-element

MIMO antenna forms a 20-element planar MIMO antenna and it is embedded at the top of the cuboid block for 3D system-in-package. Its results are almost similar to the quad-element MIMO antenna without compromising any aspect; this is another novelty in the presented proposal. The complete details about the proposed antenna are shown in the following sections.

3.2 Details of Antenna Design

3.2.1 Single-Element Antenna

The proposed MIMO antenna is designed by utilizing the design of a single antenna on the dual-layer laminated FR4-epoxy substrate (ε_r = 4.4, tan δ = 0.02, thickness = 0.8 mm) for wideband application. The design evolution of the single antenna primarily starts from a rectangular monopole antenna on a fixed cross-section of 15×15 mm^2, fed through 50Ω microstrip line and it is considered as Case 1. It covers a -10 dB bandwidth of 5.2-8.5 GHz. Generally, the larger value of electrical length is responsible for lower operating frequency. To achieve the highest operating wavelength and enhance impedance bandwidth with fixed antenna size, dual symmetric strips (a combination of L-shaped, inverted E-shaped, and right triangle loaded-stub) are connected to rectangular monopole antenna in Case 2 and it covers an enhanced -10 dB bandwidth of 5.1-9.1 GHz with dual resonating frequency. Further, a tapered microstrip line feed replaces the conventional rectangular microstrip line feed for better impedance matching and bandwidth in final Case 3. It obtained a -10 dB impedance bandwidth of 61.1% (5.0-9.4 GHz), having a peak gain value of 3.9 dBi in the wideband. The final configuration of the single antenna is shown in Fig. 3.1(a), and the *S*-parameter results of all three cases are shown in Fig. 3.1(b).

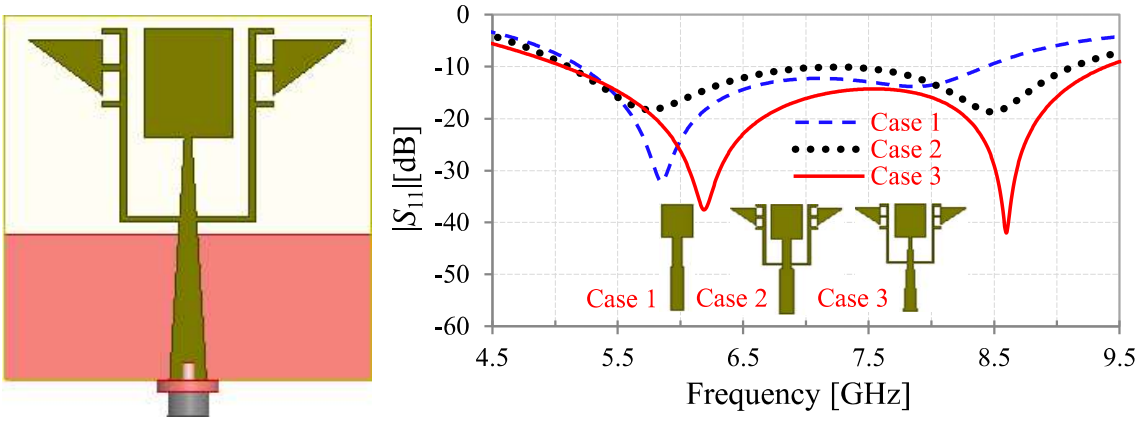

(a) (b)

Fig. 3.1: The single proposed antenna (a) configuration and (b) corresponding *S*-parameter characteristics.

3.2.2 Quad-Element MIMO Antenna

In the next step, the single antenna is placed orthogonally symmetric at the corner side of the substrate of cross-section 35×35 mm^2 (0.84λ_g×0.84λ_g, where λ_g is guided wavelength at lowest operating frequency of 3.95 GHz), forms quad-element MIMO antenna with the discrete ground plane. A minimum edge to edge separation of 6.5 mm (0.155λ_g) between antenna elements is chosen to make a compact/closely-spaced design. It provides a -10 dB impedance bandwidth of 66.95% (4.60-9.23 GHz) with a high isolation value of 17 dB between antenna elements. Further, a connecting strip (plus-shaped with meander-line) having a width of 0.2 mm (0.004λ_g) is used to make antenna shared ground plane, thereby flowing current path is increased, and electrical wavelength is also increased. Hence, the lowest operating frequency of the proposed MIMO antenna is reduced and covers 3.95-8.30 GHz without compromising the correlation between antenna elements throughout the wideband; this is the novelty of the proposed antenna. Furthermore, an optimized slit is created on each discrete ground plane due to which electrical wavelength is further increased. Hence, impedance bandwidth is further enhanced by 0.65 GHz in the frequency band (3.95-8.95 GHz) with the same isolation value. The final configuration of the quad-element MIMO with optimized dimension parameters are illustrated in Fig. 3.2.

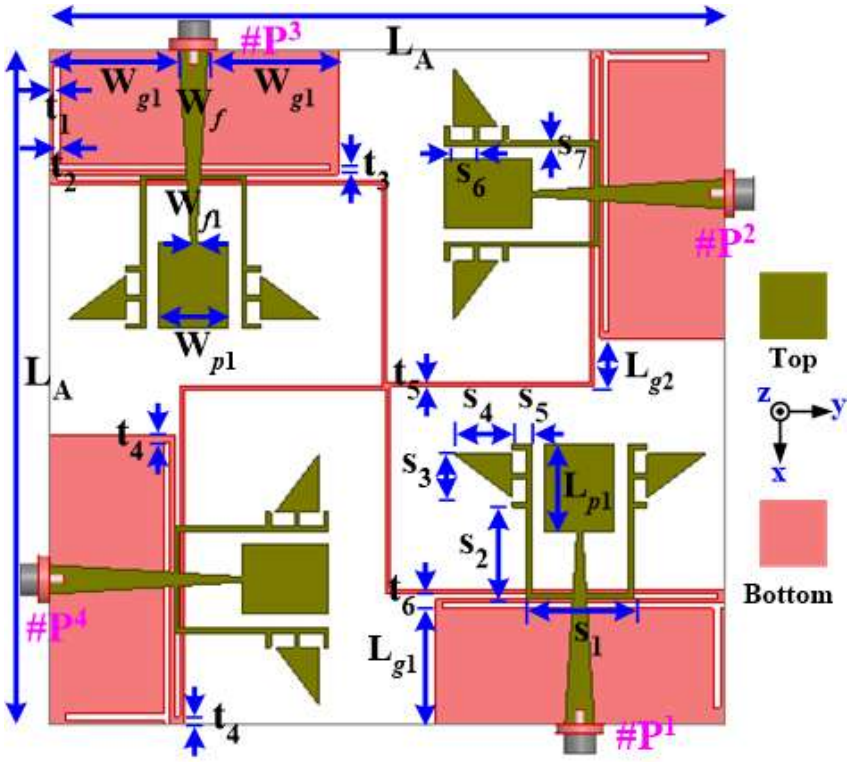

Fig. 3.2: The proposed quad-element MIMO antenna with dimension parameters. Dimensions (*in mm*): L_A=35, L_{g1}=6, L_{g2}=2.5, W_{g1}=6.75, W_f=1.5, W_{f1}=0.3, t_1=0.2, t_2=0.4, t_3=0.3, t_4=0.4, t_5=0.2, t_6=0.8, L_{p1}=4.5, W_{p1}=3.6, s_1=5.5, s_2=4.75, s_3=2.25, s_4=3, s_5=1, s_6=1.25, s_7=0.25.

Further, the shape parameters of the connecting copper strip (plus-shaped with meander-line) are optimized by using the parametric studies (optimization), as illustrated in Fig 3.3, which is utilized to make a shared ground plane. In the parametric studies, the width (t_5) of the strip is varied from 0.2 mm to 0.5 mm, and it is observed that at the lowest value of width (0.2 mm), the reflection coefficient and the coupling coefficient are much better than other values (0.3mm to 0.5 mm). Due to a minimal implementing available area and increasing complexity in the fabrication, the optimized value is not chosen to be less than 0.2 mm. Therefore, the optimized strip's width of 0.2 mm is considered; on that value, the obtained results are found most appropriate.

3.2.3 Surface Current Distribution

Fig. 3.4 shows current distribution plots on the surface of the antenna elements (top) and interconnected shared ground plane (bottom), when port_1 (#P[1]) is excited, and other

ports (#P^2, #P^3, and #P^4) are kept matched terminated through the 50Ω load. It can be easily observed that the orientation of the current is highly concentrated to boundaries of the stub and interconnecting meander-line strip respectively to the radiators and ground plane at 4.6 GHz. Still, at 8.7 GHz, the current is highly concentrated near the boundaries of the slits, along with that. The high current density on both top and bottom provides good impedance matching with a low correlation between antenna elements throughout the wideband.

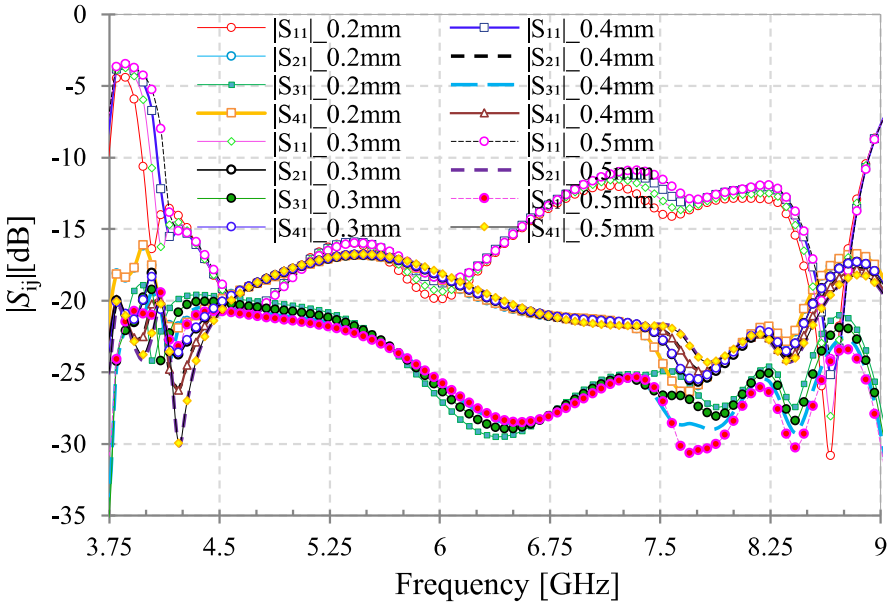

Fig. 3.3: The parametric studies on the connecting ground strip corresponding *S*-parameters characteristics.

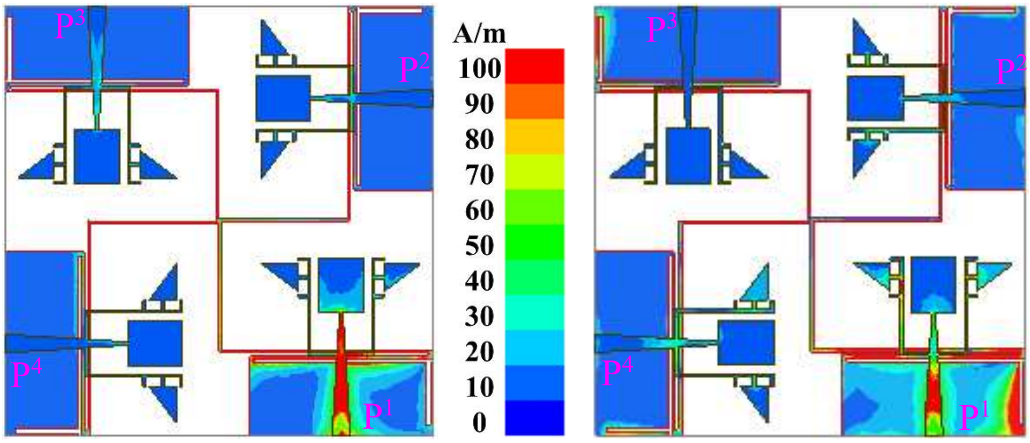

(a) (b)

Fig. 3.4: Current distribution on the surface of the antenna at (a) 4.6 GHz and (b) 8.7 GHz.

3.3 Results and Discussion

3.3.1 *S*-parameters

The prototype of the quad-element MIMO antenna (top and bottom view) and corresponding *S*-parameters are shown in Fig. 3.5(a)-(c), respectively. It has a -10 dB ($S_{ij} \in i=j$) impedance bandwidth of 78.94% (3.91-9.01 GHz) and a minimum isolation value ($S_{ij} \in i \neq j$) better than 17 dB with the close matching between the simulated and measured results, shown in Fig 3.5(c). The minor discrepancy occurred mainly due to manual fabrication and soldering tolerance. The covered wideband may be applicable in 5G Sub-6 GHz (n79), WLAN, Wi-Fi, WiMAX, and HYPERLAN/1, 2.

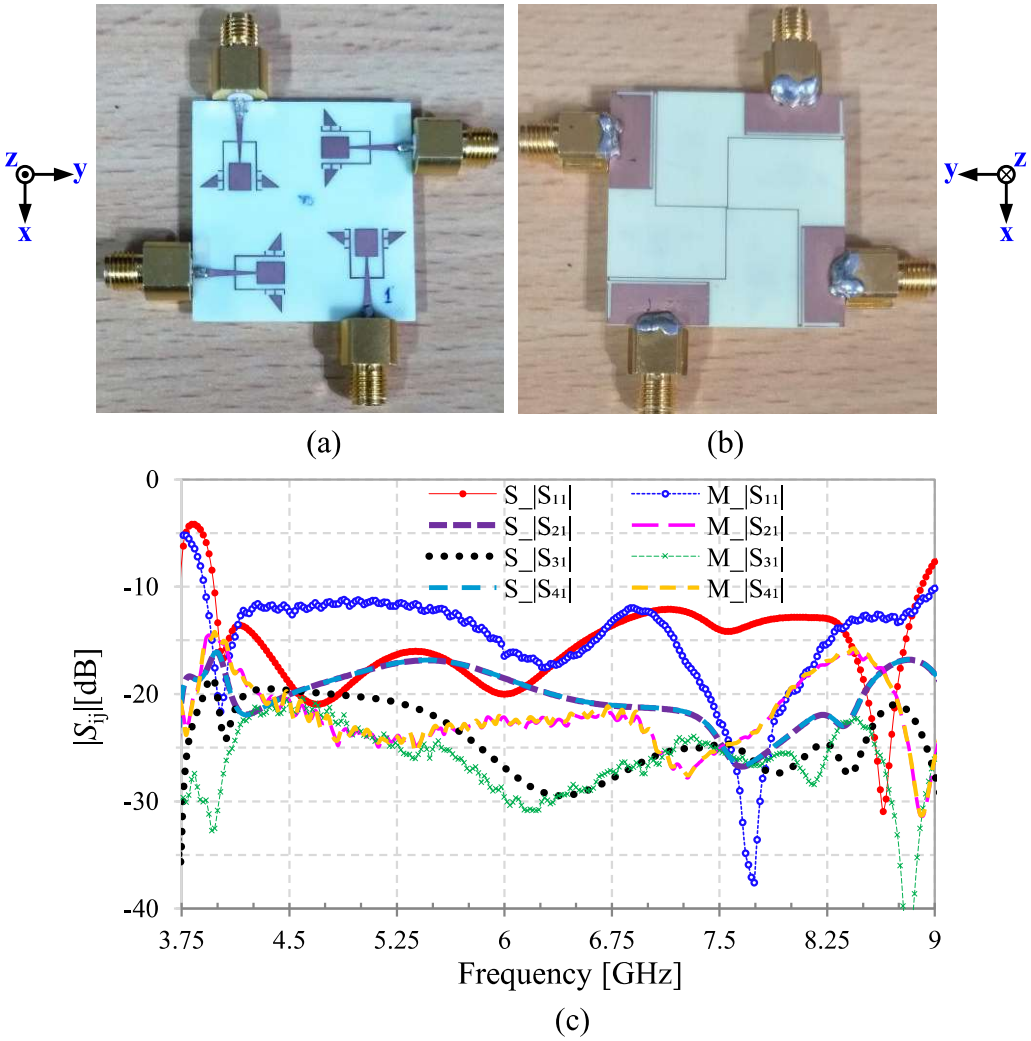

Fig. 3.5: The prototype of the quad-element MIMO antenna (a) top view, (b) bottom view, and (c) corresponding simulated and measured *S*-parameters.
Abbreviation: S = simulated, M = measured.

3.3.2 Radiation Pattern

In Fig. 3.6(a)-(b), 2-D radiation patterns of the proposed MIMO antenna are depicted, respectively, when port_1 is excited, and the other ports are kept matched terminated through 50 Ω load. The 2-D radiation patterns are plotted in two principal planes (xz and yz) at 4.6 GHz and 8.7 GHz. The measured and simulated 2-D radiation patterns are found in similitude with close omnidirectional patterns.

Fig. 3.7(a)-(b) shows 3-D omnidirectional radiation patterns at the frequency of 4.6 GHz and 8.7 GHz, when port_1 is excited, and rest all are kept matched terminated. The peak gain value of 3.97 dBi and 2.49 dBi are obtained at 4.6 GHz and 8.7 GHz, respectively.

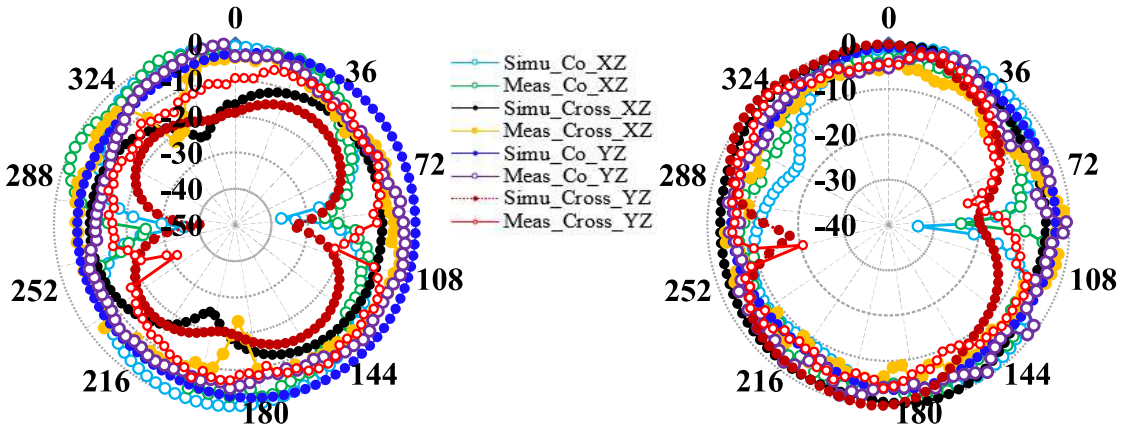

(a) (b)

Fig. 3.6: 2-D radiation patterns in xz-plane and yz-plane when port_1 is excited and other ports are kept matched terminated at (a) 4.6 GHz and (b) 8.7 GHz.

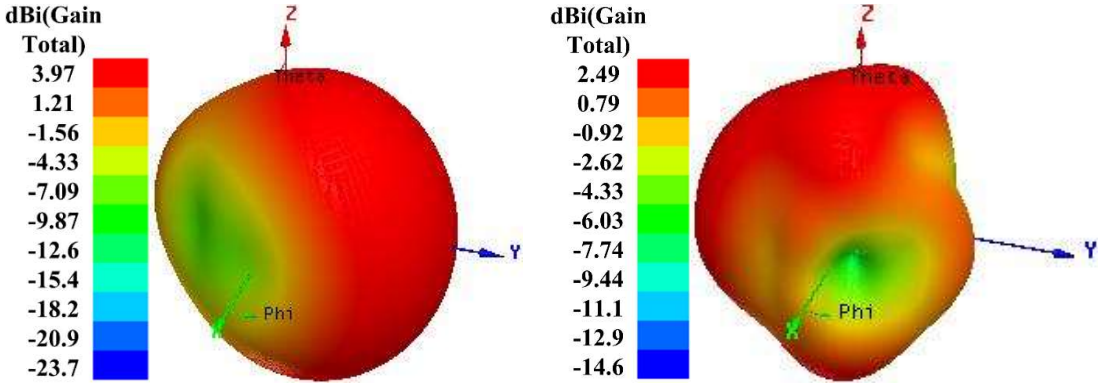

(a) (b)

Fig. 3.7: 3-D radiation patterns when port_1 is excited and other ports are kept matched terminated at (a) 4.6 GHz and (b) 8.7 GHz.

3.3.3 Efficiency and Gain

The total efficiency of the i^{th} element and multiplexing efficiency of the N-element MIMO system are approximated in [21], [25]. The approximated peak value of the radiation efficiency, total efficiency, and multiplexing efficiency are 93.2%, 89.8%, and 89.7%, respectively in the covered wideband. Similarly, the simulated and measured peak gain value are 4.52 dBi, and 4.8 dBi, respectively, as illustrated in Fig. 3.8.

3.3.4 Diversity Performances of the MIMO Antenna

The envelope correlation coefficient (ECC), total active reflection coefficient (TARC), and channel capacity loss (CCL) are approximated in [27], [28], [30].

3.3.4.1 ECC

The simulated and measured plots of ECC are depicted in Fig. 3.9(a). The simulated ECC results are obtained by using both *S*-parameters and 3-D complex field equation. Whereas, the measured results of the ECC are calculated by using *S*-parameters only. A maximum value of ECC is 0.251 but from 4.0 to 9.0 GHz, the values are well below 0.008.

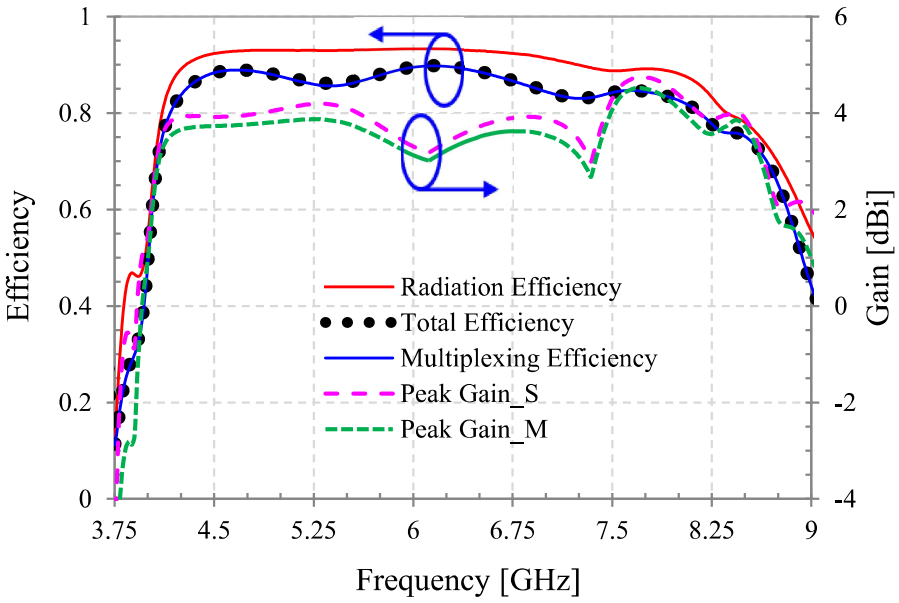

Fig. 3.8: Efficiency and gain of the quad-element MIMO antenna.
Abbreviation: S = simulated, M = measured.

3.3.4.2 TARC and CCL

The TARC is estimated by exciting port_1 at unity amplitude and zero phase ($P^1=0^\circ$), while other port_2, 3, and 4 are excited by similar amplitude but different phases (varied from 0° to 360°) in five different cases, that is,

Case-1: $P^2=0^\circ$, $P^3=60^\circ$, $P^4=120^\circ$, Case-2: $P^2=60^\circ$, $P^3=120^\circ$, $P^4=180^\circ$, Case-3: $P^2=120^\circ$, $P^3=180^\circ$, $P^4=240^\circ$, Case-4: $P^2=180^\circ$, $P^3=240^\circ$, $P^4=300^\circ$, Case-5: $P^1=0^\circ$, $P^2=240^\circ$, $P^3=300^\circ$, $P^4=360^\circ$.

A maximum value (simulated and measured) of TARC and CCL are 0.34 and 0.65 bits/s/Hz, respectively, in the operating wideband for quad-element MIMO antenna, as illustrated in Fig. 3.9(b).

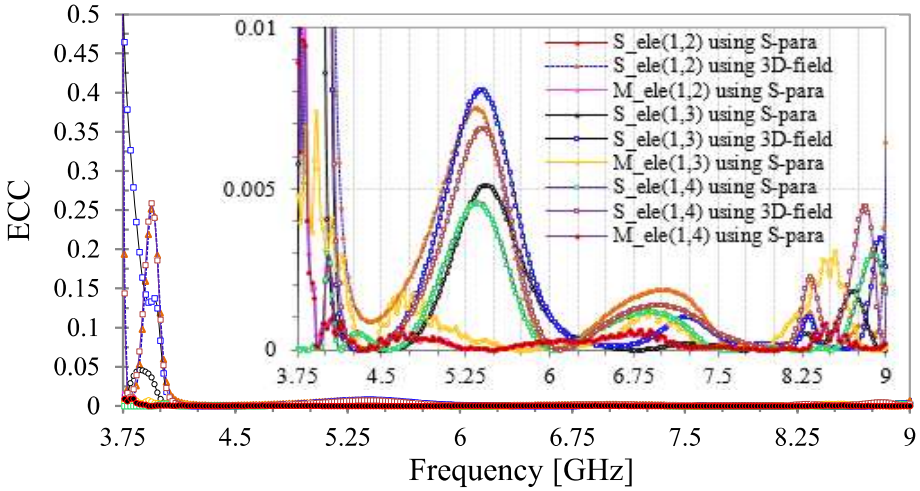

(a)

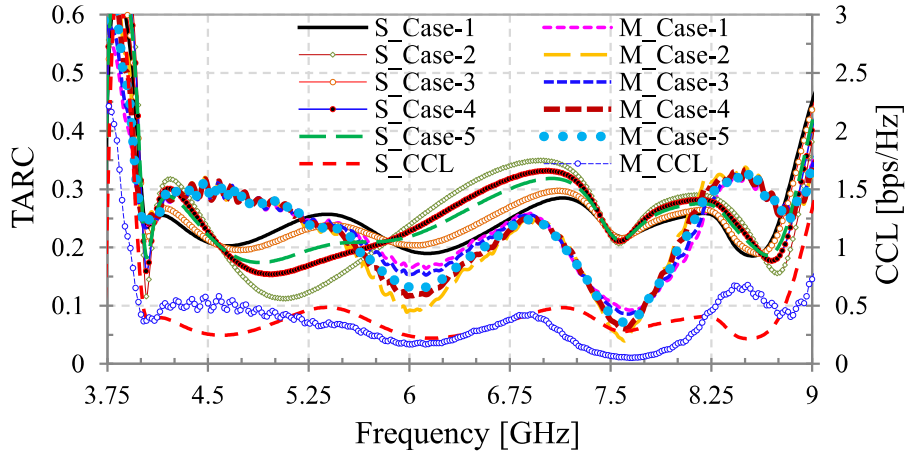

(b)

Fig. 3.9: (a) ECC and (b) TARC and CCL for quad-element MIMO antenna. Abbreviation: S = simulated, M = measured.

3.3.5 Comparison and Review

To justify the advantages and issues considering the table data, the proposed quad-element MIMO antenna is compared with the previous proclaimed articles, as listed in Table 3.1. However, the design in [71] and [72] have occupied a smaller electrical area and overall volume than the proposed antenna but they are suffering from a low isolation value, along with the design in [71] have a larger impedance bandwidth. Therefore, based on the obtained performances, the proposed quad-element MIMO antenna is the more desirable and suitable for extending higher-order MIMO antenna.

3.4 The 3D-MIMO Antenna System

3.4.1 20-Element MIMO Antenna Configuration

The proposed quad-element MIMO antenna is utilized as a unit cell for configuring a planar 20-element MIMO antenna. The four-unit cell (quad-element MIMO antenna) are orthogonally placed around the corner of another unit cell. The minimum distance between the two-unit cell corner is $5\sqrt{2}$ mm ($0.169\lambda_g$) and the grounds of them is connected through a 0.2 mm thick copper strip to make shared antenna ground. To reduce the coupling between adjacent elements i.e., element-1 and element-8, the distance between unit cell corner and width of the copper strip are optimized. Further, the proposed 20-element MIMO antenna is embedded at the top face of a cubic block having dimensions of $115\times115\times35$ mm^3 forms a 3D-MIMO antenna system. The material of the block is selected polystyrene having relative permeability (ε_r) of 2.6 [119]. The rectangular block area with 0.8 mm height between two corner unit cell is attached with the antenna substrate through a bonding material (glue) having an approximate thickness of 0.017 mm. This type of MIMO antenna can be utilized in localization system where high-speed receptions are desired. The complete geometry of the 3D-MIMO system and optimized parameters are depicted in Fig. 3.10.

Table 3.1: Comparison of the proposed antenna with similar MIMO antenna

Ref.	f_0	T_A	T_V	P_G	IBW	I_{min}	G_C	ECC
[112]	3.3	0.70863	14.2031	2	24 (-6 dB)	10	Y	0.06
[112]	2.45	0.44838	10.6754	2.9/5.4	14.4/20.3	17/22	Y	0.11/0.16
[75]	3.4	1.06608	35.2241	4.3	11.11	11.5	Y	0.09
[72]	2.7	0.43027	11.2894	4	58.64	11	Y	0.07
[71]	2.2	0.36154	7.7295	4	96.23	14	N	0.25
[68]	1.8	1.96560	34.0179	6.4	46.81	15	Y	0.12
Pro.	3.95	0.70505	13.5319	4.8	77.52	17	Y	0.25

T_A = total electrical area in λ_g^2, $\lambda_g = c/f_0\sqrt{\varepsilon_{eff}}$ being guided wavelength at lowest operating frequency (f_0 in GHz), ε_{eff} is effective relative permittivity of the substrate as mentioned in [80], T_V = total antenna electrical volume in $10^{-3}\lambda_g^3$, P_G = peak gain in dBi, IBW = -10 dB impedance bandwidth in %, I_{min} = minimum isolation in dB, G_C = common ground, Y = Yes, N = No.

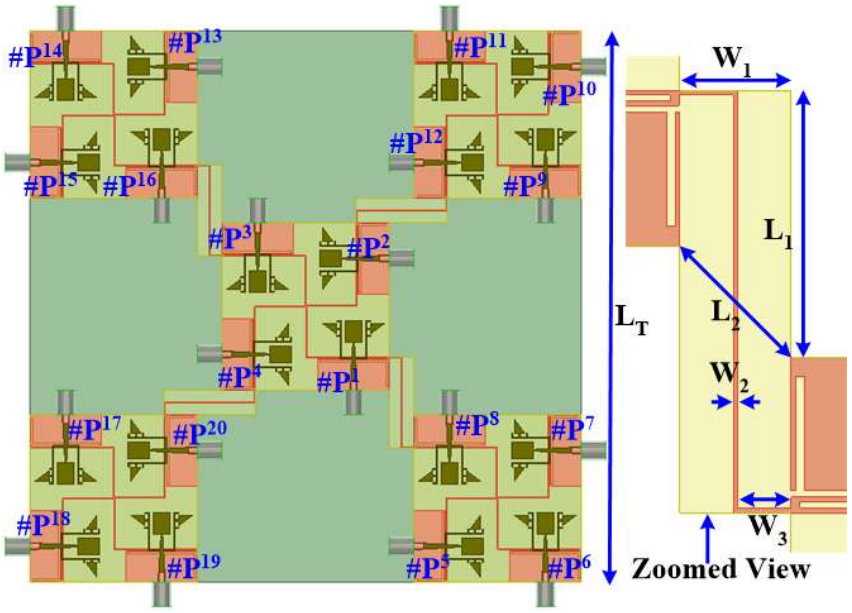

(a)

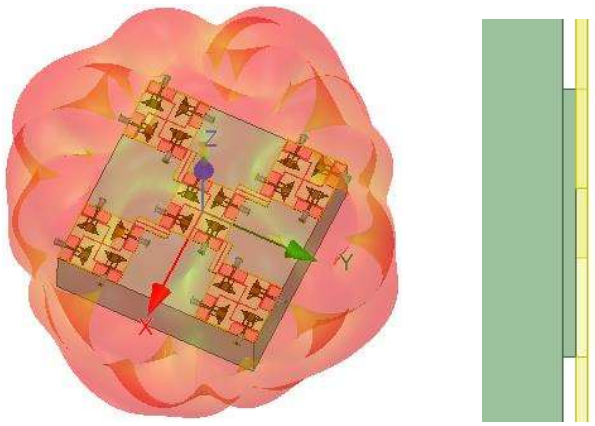

(b) (c)

Fig. 3.10: 20-element 3D-MIMO antenna (a) configuration with parameters (b) 3D-view with 3-D radiation pattern, and (c) side-view.
Dimensions (*in mm*): L_T=115, L_1=12, L_2=5√2, W_1=5, W_2=0.2, W_3=2.4.

3.4.2 Results and Discussion

3.4.2.1 *S*-parameters

All reflection coefficients are not identical, mainly due to extra loading of the substrate and connecting ground strip between two corners of the quad-element MIMO antenna. The reflection coefficient S_{11} is identical to S_{22}, S_{33}, S_{44}. Similarly, S_{55}, S_{66}, S_{77}, and S_{88} are identical to (S_{99}, S_{1313}, S_{1717}), (S_{1010}, S_{1414}, S_{1818}), (S_{1111}, S_{1515}, S_{1919}), and (S_{1212}, S_{1616}, S_{2020}), respectively, which means all reflection coefficients are identical to S_{11}, S_{55}, S_{66}, S_{77}, and S_{88}. All other transmission coefficients are similar to the S_{12}, S_{13}, S_{14}, S_{15}, S_{16}, S_{17}, and S_{18}. The S-parameter characteristics of the 20-element MIMO antenna system are plotted in Fig. 3.11(a). As seen, the results show that it has a minimum -10 dB (S_{11}, S_{55}, S_{66}, S_{77}, and S_{88}) impedance bandwidth of 4.15-8.25 GHz and a minimum isolation value ($S_{ij} \in i \neq j$) better than 17 dB without any decoupling circuit. The S-parameter results of the 20-element MIMO antenna system slightly deviate from the quad-element MIMO antenna, still satisfactory for 3D system-in-package. The prototype and measured results are not demonstrated here due to brevity. The simulated results confirm that it can be a competent candidate for indoor localization systems and WPAN application-based practical devices.

3.4.2.2 Efficiency and Gain

The approximated peak values of the radiation efficiency for element-1, 5, 6, 7, and 8 of the 3D-MIMO system are 93.3%, 94.1%, 93.5%, 93.3% and 93.2%, respectively, in the covered wideband. Similarly, peak gain values are 7.92 dBi, 9.88 dBi, 9.28 dBi, 9.36 dBi, and 8.1 dBi, respectively, as illustrated in Fig. 3.11(b). As seen, the radiation efficiency values are almost similar, and the values of gain are improved throughout the wideband compared to single antenna and quad-element MIMO antenna.

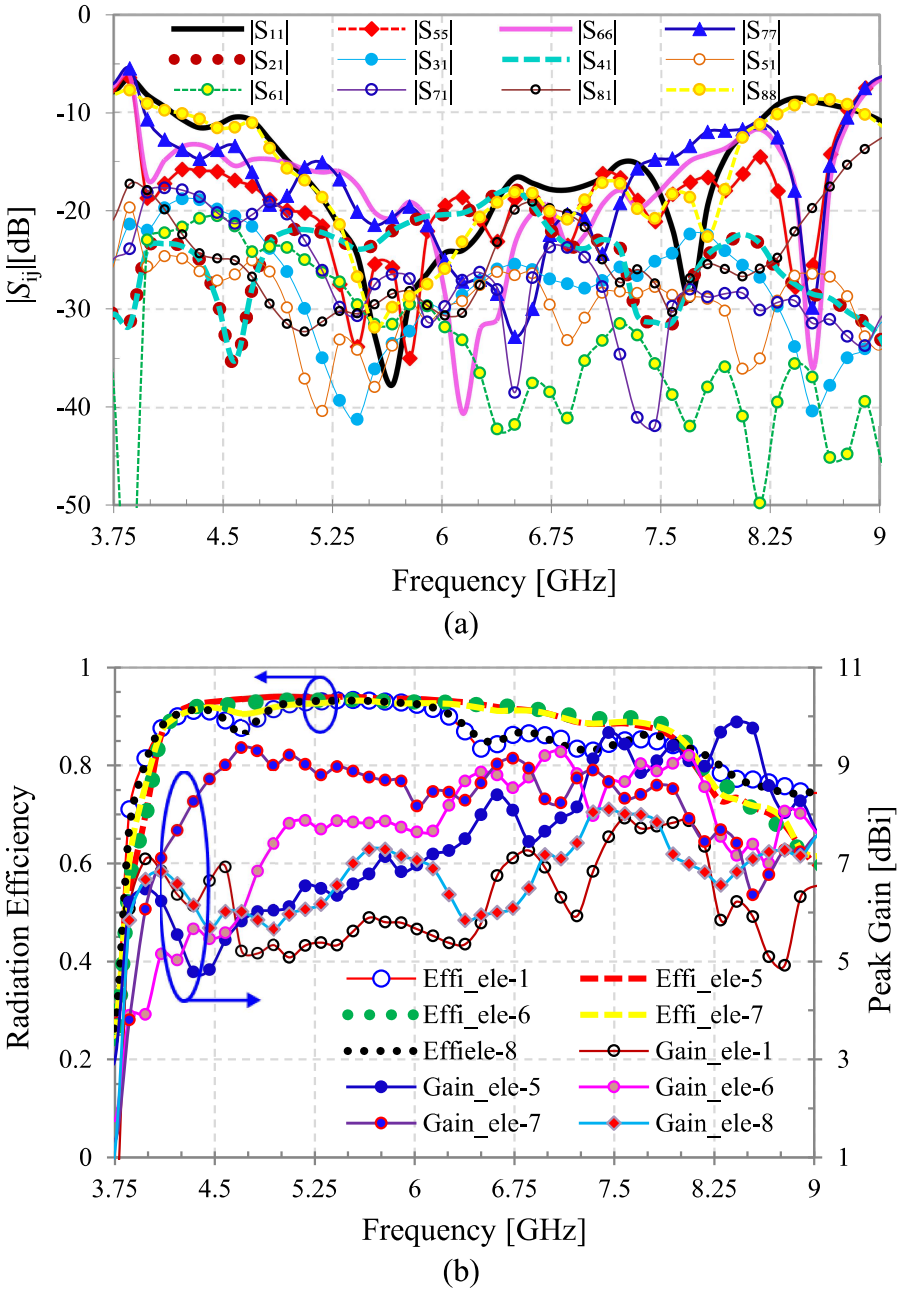

Fig. 3.11: 20-element 3D-MIMO antenna, corresponding (a) *S*-parameters and (b) radiation efficiency and peak gain.

3.4.2.3 Comparison Review with 3D-MIMO Antenna

To justify the advantages and issues considering the table data, the proposed quad-element MIMO antenna is compared with the previous proclaimed articles, as listed in Table 3.2. However, the design in [119] and [120] have single antenna element and PCBs of them arranged around the cubic and octagonal shaped 3D polystyrene body to configure MIMO antenna, still have discrete ground plane. Similarly, in [121], two-

element antenna arranged around the octagonal shaped 3D polystyrene body. They have a larger isolation value compare to proposed antenna but suffering from a smaller number of antenna element in the MIMO antenna. Therefore, based on the obtained performances, the proposed 20-element 3D-MIMO antenna is the planar structure based more desirable antenna which is suitable for localization system.

Table 3.2: Comparison of the proposed 20-element MIMO antenna to similar non-planar 3D-MIMO antenna

Ref.	$T_{E\text{-}PS}$	$P_{D\text{-}PS}$	$T_{E\text{-}NPS}$	$P_{D\text{-}NPS}$	G_C	IBW	I_{min}
[119]	1	32×36×1.5	4	1156×36	No	3.1-10.6	20
[120]	1	28×23×1.5	8	3017.77×32	No	3.1-10.6	20
[121]	2	36×22×1.5	16	2554.24×36	Yes	3.35-3.65	28
Pro.	4	35×35×0.8	20	13225×35.8	Yes	4.15-8.25	17

$T_{E\text{-}N}$ = total number of elements–planar structure, $T_{E\text{-}NP}$ = total number of elements–non planar structure, IBW = -10 dB impedance bandwidth in GHz, I_{min} = minimum isolation in dB, G_C = common ground, $P_{D\text{-}P}$ = physical dimension in mm×mm×mm–planar structure, $P_{D\text{-}NP}$ = physical dimension in mm^2×mm–non planar structure. *Area of regular octagon = $[L^2(1+\sqrt{2})^2 - 4\times1/2\times(L/\sqrt{2})^2]$, L is side length of the octagon.

3.5 Summary

The proposed wideband MIMO antenna in this chapter is the most appropriate (based on table data) compared to other recent reported designs in Tables 3.1 and 3.2. In Table 3.2, the reported literature has better isolation, but they suffered from fewer antenna elements. The use of a separate ground plane is not convenient in many practical applications [122]. The proposed antenna has a minimal footprint and high isolation without any decoupling network with a shared ground plane. The obtained results (isolation, gain, efficiency, pattern, ECC, TARC, and CCL) in the wideband are satisfactory. Hence, the proposed extremely compact quad-element MIMO antenna is utilized to construct a 20-element 3D-MIMO system, which can be appropriate for WPAN, indoor localization system, 3D system-in-package application-based compact devices.

After implementation of 20-element MIMO antenna by utilizing four-element MIMO antenna, a compact ultra-wideband eight-element MIMO antenna is presented in next Chapter 4. By utilizing that, a novel 32-element MIMO antenna is proposed for IoV based automotive vehicles, ensuring highly improved performances compared to this chapter.